Cholesterol Promotes Hemifusion and Pore Widening in Membrane Fusion Induced by Influenza Hemagglutinin

Subrata Biswas, Shu-Rong Yin, Paul S. Blank, and Joshua Zimmerberg

Laboratory of Cellular and Molecular Biophysics, Eunice Kennedy Shriver National Institute of Child Health and Human Development, National Institutes of Health, Bethesda, MD 20892

Cholesterol-specific interactions that affect membrane fusion were tested for using insect cells; cells that have naturally low cholesterol levels (<4 mol %). Sf9 cells were engineered (HAS cells) to express the hemagglutinin (HA) of the influenza virus X-31 strain. Enrichment of HAS cells with cholesterol reduced the delay between triggering and lipid dye transfer between HAS cells and human red blood cells (RBC), indicating that cholesterol facilitates membrane lipid mixing prior to fusion pore opening. Increased cholesterol also increased aqueous content transfer between HAS cells and RBC over a broad range of HA expression levels, suggesting that cholesterol also favors fusion pore expansion. This interpretation was tested using both trans-cell dye diffusion and fusion pore conductivity measurements in cholesterol-enriched cells. The results of this study support the hypothesis that host cell cholesterol acts at two stages in membrane fusion: (1) early, prior to fusion pore opening, and (2) late, during fusion pore expansion.

The Journal of General Physiology

INTRODUCTION

Successful infection by influenza virus requires that the envelope spike protein, hemagglutinin (HA), catalyzes fusion between the viral envelope and the intracellular endosomal membrane of the target cell and creates a pore large enough to release the viral genome. There is a growing appreciation that membrane lipids play a role in this critical event, coming mostly from experiments and theory on lipid composition in relationship to membrane monolayer curvature stress (Markin et al., 1984; Kozlov et al., 1989; Chizmadzhev et al., 1995; Chernomordik, 1996; Siegel, 1999; Kuzmin et al., 2001; Kozlovsky and Kozlov, 2003; Chernomordik et al., 2006). Recently there has been consideration given to the role of membrane phase behavior and membrane microdomains on the lateral distribution, sorting, and interactions of lipids with membrane proteins in general, and viral envelope glycoproteins in particular (Brown and London, 1998; Wang et al., 2001; Suomalainen, 2002; Chazal and Gerlier, 2003; Edidin, 2003; Schmitt and Lamb, 2004; Hess et al., 2005). Cholesterol is a major and vital constituent of eukaryotic cell membranes. Its unique structure, a small hydrophilic head group and rigid, hydrophobic, fused rings, favors preferential association with saturated acyl-chain lipids and sphingolipids to form liquid-ordered microdomains (termed lipid "rafts") in phospholipid bilayer membranes of the right composition (Fridriksson et al., 1999; Zhang et al., 2000; Feigenson and Buboltz, 2001). Lipid rafts are hypothesized to exist in the cell plasma membrane (Simons and Ikonen, 1997) at specialized sites where proteins, having favorable associations with the ordered, cholesterol-rich environment, are concentrated (Scheiffele et al., 1997; Brown and London, 1998; Kenworthy et al., 2000).

In support of an important role for membrane microdomains are experiments validating one prediction of the lipid raft theory: biological function mediated by the putative raft protein should be changed when rafts are altered by a reduction in membrane cholesterol (McGee et al., 1996; Scheiffele et al., 1997; Simons and Ikonen, 1997; Harder et al., 1998; Keller and Simons, 1998; Fridriksson et al., 1999; Churchward et al., 2005). For viruses, lipid rafts have been proposed to act at the stages of binding or fusion. The cell surface receptors of a few enveloped and nonenveloped viruses colocalize, by microscopy, with markers for raft components (cholera toxin binds to gangliosides) and partition into floating fractions of detergent extracts of cells (called detergent-insoluble or -resistant membranes, DRM) (Kozak et al., 2002; Popik et al., 2002; Stuart et al., 2002; Ashbourne Excoffon et al., 2003). If rafts exist with finite, "small" dimensions, then receptors could concentrate in "small" patches of membrane, increase their local density, and enhance viral interactions with the host cell, promoting productive viral entry (Danieli

Correspondence to Joshua Zimmerberg: Joshz@helix.nih.gov

S. Biswas' present address is Division of Cardiology, Johns Hopkins University School of Medicine, Baltimore, MD 21205.

The online version of this article contains supplemental material.

Abbreviations used in this paper: CF, carboxy fluorescein; COD, cholesterol oxidase; GPI, glycosylphosphatidylinositol; HA, hemagglutinin; MβCD, methyl-β-cyclo dextrin; RBC, red blood cells; RFI, relative fluorescence intensity; TMD, transmembrane domain.

The Rockefeller University Press $30.00
J. Gen. Physiol. Vol. 131 No. 5 503–513
www.jgp.org/cgi/doi/10.1085/jgp.200709932

et al., 1996; Viard et al., 2002). Additionally, fusogenic proteins associate with lipid rafts on the viral surface. Influenza virus, some retroviruses, and filoviruses use cholesterol-rich membrane microdomain sites for assembly and cell entry (Ono and Freed, 2001; Bavari et al., 2002; Del Real et al., 2002; Guyader et al., 2002; Sun and Whittaker, 2003; Takeda et al., 2003). The influenza virus HA transmembrane domain (TMD) associates with DRM; when expressed in cells, mutations in the TMD and in the HA cytoplasmic tail show reduced association with detergent-insoluble glycolipid complexes (Scheiffele et al., 1997; Lin et al., 1998; Scheiffele et al., 1999). Cholesterol-depleting agents like methyl-β-cyclo dextrin (MβCD) disrupt detergent-resistant membrane localization of these viral proteins and reduce infectivity and fusion activity (Sun and Whittaker, 2003; Takeda et al., 2003). Influenza and Semliki Forest virus each requires cholesterol and sphingolipids in the target membrane for fusion pore expansion (White and Helenius, 1980; Kielian and Helenius, 1984; Phalen and Kielian, 1991; Nieva et al., 1994; Raznikov and Cohen, 2000).

While the raft theory predicts a cholesterol dependence of certain biological processes, there may be other explanations that remain untested. In particular, a recent report on influenza virus shows that depletion of cholesterol alters the phase behavior of the viral envelope in the direction of an increased fraction of gel phase lipids, which may hinder HA mobility and thereby explain inhibition of fusion upon cholesterol extraction (Polozov et al., 2008). Alternatively, membrane lipid components may interact directly with fusion intermediates. Although cholesterol has a negative spontaneous monolayer curvature, it is hard to estimate this effect on membrane curvature because the amount of curvature stress introduced by cholesterol is a function of the other phospholipids surrounding it (Huang and Feigenson, 1999). However, cholesterol is expected to promote and stabilize the local bilayer bending that is hypothesized to take place during membrane fusion, since the curvature stress is in the direction of negative curvature (Markin et al., 1984; Kozlov et al., 1989; Chizmadzhev et al., 1995; Chernomordik, 1996; Siegel, 1999; Raznikov and Cohen, 2000; Haque et al., 2001; Kuzmin et al., 2001; Kozlovsky and Kozlov, 2003; Zimmerberg and Kozlov, 2006). Indeed, experiments on the exocytosis of sea urchin eggs indicate a role for cholesterol, in part, due to its negative spontaneous curvature (Churchward et al., 2008). Alternatively, cholesterol may bind directly to membrane proteins and change their conformation, or direct protein folding during conformational changes along a specific pathway.

Despite the demonstrated association of HA with cholesterol-rich domains and a reduction in virus infectivity with cholesterol depletion, it is not clear at what stage of fusion cholesterol acts, nor how cholesterol affects the fusion pore. In this study, the role of cholesterol at different stages of fusion was determined. Insect cells, which have no measurable sphingolipids and little cholesterol (Marheineke et al., 1998), are suitable for hemagglutinin expression, can be enriched with cholesterol (Gimpl et al., 1995), and fuse to labeled red blood cells (RBC) that have their normal complement of cholesterol (Kretzschmar et al., 1995; Latham and Galarza, 2001; Plonsky et al., 2008). Cholesterol enrichment of insect cells facilitated both lipid mixing and fusion pore expansion up to levels similar to those observed between mammalian cells expressing HA and RBC. This suggests that cholesterol (a) promotes the formation and growth of the contact sites between membranes that allow lipid mixing and (b) helps to expand the fusion pore and thereby increases the efficiency of fusion.

MATERIALS AND METHODS

Construction of HA Expression Vector

The full-length DNA sequence encoding X31 HA (ecto, transmembrane, and cytoplasmic domains) flanked by NotI (5' end) and Xba I (3' end) restriction sites was produced by PCR. The additional stop code (TAA) to the 3' end of the cytoplasmic domain was followed by the original stop codon TGA in order to prevent V5 and 6 His tags in the expression vector from fusing into HA. The fragment was inserted into the corresponding restriction site of pIZ/V5-His expression vector (Invitrogen). The plasmid was called pHA2. X31 HA DNA sequence was also inserted into another vector (pIZT/V5-His, Invitrogen) containing the GFP sequence fused to antibiotic Zeocin binding protein "ble" called pHA1. For glycosylphosphatidylinositol (GPI)-HA, fragment nucleotide from the template pTM1-HAx31-GPI plasmid (gift from J. White, University of Virginia School of Medicine, Charlottesville, VA) was amplified in PCR using a forward primer containing BamHI site 5'-GCG GAT CCA TGA AGA CCA TCA TTG CTT TGA GC-3' and a backward primer containing NotI site 5'-ATG CGG CCG CGG TGT GCT AAG AAT GTG ATT CC-3' and the fragment was inserted into the corresponding restriction site of a pIZ expression vector (Invitrogen) called pGPI-HA. All the inserts were confirmed by DNA sequencing.

Cell Culture and Stable Cell Line Development

Sf9 cells (Invitrogen) were maintained according to the Invitrogen manual, and transfected using the calcium phosphate transfection kit (Invitrogen) using 0.1–10 μg of DNA. Cells were used 48 h after transfection. After transient transfection of Sf9 cells, surface expression of HA was detected using FITC-conjugated anti-HA mAb (Fig. 1 a). In addition to epitope exposure, transfection also made the cells competent to fuse to RBC at 30°C and pH 4.9 (Plonsky et al., 2008). To minimize HA expression variability, cells were selected for a cell line named "HAS" cells. For stable expression, transfected cells were selected with 800 μg/ml of Zeocin (Invitrogen) and the expression of the HA was successfully maintained in the presence 200 μg/ml Zeocin concentration for 2 mo. HAS cells stably express HA on their surface, as demonstrated by cell surface biotinylation and immunoblot assay (Fig. 1 b). Flow cytometry of immunolabeled HAS cells showed HA expression to be $4.3 \pm 1.3 \times 10^5$ ($n = 5$) copies of HA per cell. Using beads of calibrated antibody binding capacity we estimate that $18 \pm 1\%$ of HAS cells have $\sim 1{,}630 \pm 30$ ($n = 5$) copies of HA molecules per μm^2 of cell surface; this is comparable to the HA densities of transfected Sf9 cells (Fig. 1). Thus, HAS cells express biologically active, fusion-competent HA. HAS cells were then frozen, and thawed cells from passage 3 to 30 were used.

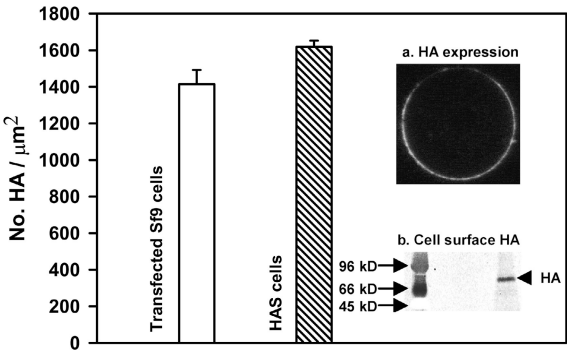

Figure 1. Influenza HA expression in Sf9 insect cells. Bar (with pattern) represents the estimated number of cell surface HA molecules in HAS cells. The HA expression level of HAS cells was determined by the number of molecules of fluorescent conjugated antibody HC3 (anti-HA mAb) bound per cell, by flow cytometry. The mean fluorescence intensities (MFI) of the FITC-conjugated HC3 bound to HAS cells, were linearly related to the mean number of mAb binding sites/cell (details in Materials and methods). ~19% of cells have ~1.63×10^3 copies of HA molecules/μm^2 ($n = 5$). (Inset a) Confocal image of FITC-conjugated HC3 stained Sf9 cells expressing HA. (Inset b) Stable HA-expressing HAS cells were surface biotinylated and lysed. HA was immunoprecipitated and biotinylated HA was recovered with protein A agarose beads. Biotinylated protein complex was separated by 10% SDS-PAGE and surface HA expression was detected by FITC-conjugated Avidin. Detection of cell surface HA expression in HAS cells indicated that insect cells are suitable for stable expression of influenza HA.

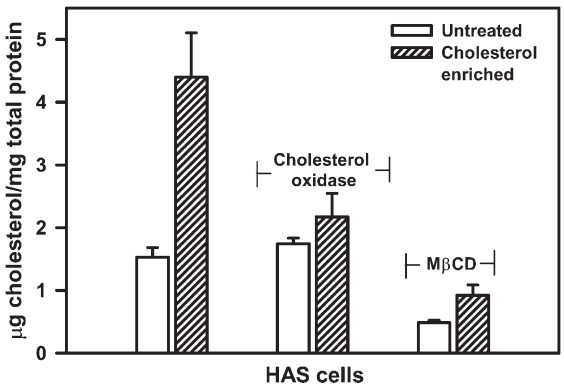

Figure 2. Loading HAS cells with cholesterol. HAS cell cholesterol was enriched by incubating cells with 1 ml cholesterol-MβCD complex (1:10, cholesterol: MβCD molar ratio) for 10 min at 30°C. Total cell lipids were extracted by 1:1 methanol:chloroform. Total cell free cholesterol (without cholesterol ester) of control cells and of cholesterol-MβCD–treated cells was determined by Amplex Red method and expressed in μg/mg of total left over cell protein after lipid extraction. Cholesterol oxidase treatment of cells, which lowered membrane-free cholesterol by oxidation, gave a reasonable estimate of free cholesterol available at the membrane. Membrane cholesterol oxidation was achieved by incubating cells with the enzyme cholesterol oxidase (COD) and 700 U of catalase, for 10 min at 30°C. Another way used to lower membrane cholesterol was to extract it from membranes using MβCD. For extraction of membrane cholesterol, cells were incubated with 10 mM MβCD in Sf9 culture medium (without FBS) for 10 min at 30°C. Thus HAS cells can be enriched with cholesterol and, alteration of the cholesterol level after enrichment with COD and MβCD treatments indicates, loaded cholesterol was in HAS membrane. (values: mean ± SEM, $n \geq 5$).

Immunoprecipitation and Western Blots

HAS cells and Sf9 cells (control cells) were biotinylated with EZ-Link NHS-LC-biotin (Pierce Biotechnology, Inc.). The cells were then lysed in lysis buffer (50 mM HEPES, 1% NP-40, pH 7.5) containing 20 μl protease inhibitor cocktail (Roche) and clarified by centrifugation. HA was immunoprecipitated with anti-hemagglutinin (X-31) mAb (a gift from J. Skehel, MRC National Institute for Medical Research, London, UK) whereas antibiotic Zeocin binding protein "ble" (Cycle 3 GFP tagged) immunoprecipitated with primary antibody anti-GFP antiserum (Sigma-Aldrich), and with protein-A agarose (GE Healthcare). Immunoprecipitated proteins were separated by SDS-PAGE and transferred to 0.22-μm PVDF membrane (Invitrogen). For HA detection, blots were probed with fluorescein-conjugated Avidin (Pierce Biotechnology), while "ble" detection blots were probed with goat anti–rabbit FITC-conjugated IgG (Sigma-Aldrich).

Cholesterol Enrichment of HAS Cells

Total cell free cholesterol concentrations were estimated using Amplex Red reagent (Molecular Probes) according to the manufacturer's protocol, except that the enzyme cholesteryl estrase was not used; the total concentration of free cholesterol, in the absence of cholesterol esters, was measured. Complexes of cholesterol (Avanti Polar) and oleic acid (trans-9-octadecenoic acid; Sigma-Aldrich) with MβCD (Sigma-Aldrich) were prepared according to Christian et al. (1997). For enrichment, trypsinized cells were incubated with 1 ml of MβCD-cholesterol or MβCD-oleic acid PBS for 10 min at 30°C before binding to RBC. To determine the degree of cholesterol enrichment using MβCD, cell cholesterol (without cholesterol esters) was measured. Total free cholesterol increased threefold after our standard preincubation (10 min, 80 μg of soluble cholesterol), from 1.5 ± 0.1 μg ($n = 5$) cholesterol per mg of total HAS cell protein to 4.4 ± 0.7 μg ($n = 5$) cholesterol per mg HAS cell protein (Fig. 2). Based on the values reported by Marheineke et al. (1998) and Gimpl et al. (1995), this enrichment corresponded to an increase from ~0.04 to ~0.12 wt:wt% cholesterol:lipid. Furthermore, the membrane cholesterol level was decreased using the enzyme cholesterol oxidase (COD). COD treatment of cholesterol-enriched HAS cells restored cholesterol levels close to control (2.2 ± 0.4 μg cholesterol per mg total HAS cell protein, $n = 5$). MβCD treatment of cholesterol-enriched HAS cells also reduced total free cell cholesterol level to 0.9 ± 0.1 μg ($n = 4$) per mg of total HAS cell protein. These results indicate that treating cells with cholesterol complexed with MβCD increased a dynamic pool of cellular cholesterol that circulated through the plasma membrane since it had access to both MβCD and COD.

Flow Cytometry

HAS (without GFP), Sf9 cells, and quantum Simply Cellular microbead standards with known antibody binding capacity beads (Bangs Laboratories) were labeled to saturation with FITC-conjugated anti-HA mAb HC3 (gift from J. Skehel). The instrument (BD LSR II) was calibrated using FITC microbead standards (Bangs Laboratories) with known molecules of equivalent soluble fluorochrome (MESF), and expression level was determined using manufacturer's protocol. Surface expression of GPI-HA was then measured using flow cytometry and compared with the known HA surface expression of HAS cells.

Confocal Microscopy

FITC-conjugated anti-HA mAb stained cells (without GFP) were layered on black ΔT dishes (Bioptecs Inc.) and observed with a Leica DMIRB confocal microscope with an FITC filter set, oil immersion

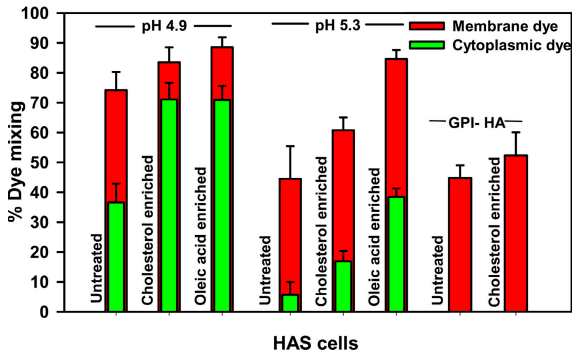

Figure 3. HAS cell cholesterol level modulates fusion activity. Double-labeled RBC (DiI C-18 and carboxy fluorescein, CF) were bound to HAS and GPI-HAS cells, and fusion triggered by application of a pH 4.9 solution for 2 min at 30°C. Cells were then incubated with pH 6.4 impermeant buffer, and the percentage of bound cells showing lipid dye transfer and cytoplasmic dye transfer were counted in a fluorescence microscope. Cholesterol and oleic acid enrichments were achieved as described in Materials and methods. Cholesterol mimics oleic acid in modulating fusion of HAS cells at the pH optima but not at pH 5.3. Cholesterol did not modulate fusion of GPI-HAS.

objective (100×/1.4-0.7 oil, PL APO Leica); images were acquired with Scanware software.

Fusion Assay

Fusion was assayed by transfer of fluorescent dye to HAS cells from double-labeled RBCs (DiI C-18 and carboxy fluorescein; Sigma-Aldrich) with some modification of previously reported protocols (Ellens et al., 1989; Chernomordik et al., 1998). For DiI the labeling protocol was modified. 4 µl of DiI (1 mg/ml in methanol) was rapidly injected into a washed RBC suspension (~150 µl packed cell volume in 500 µl of PBS w/o Ca^{2+}) under slow vortex and incubated at room temperature for 10 min. The labeled cells were diluted with 5 ml of PBS and 2.5 ml of chilled FBS and incubated on ice for 10 min. Labeled cells were washed three times in PBS and transferred to another tube and again incubated on ice for 10 min while suspended in 5 ml PBS and 2.5 ml FBS and washed five times with PBS. The labeled cells were used for binding to host cells. Trypsinized, cholesterol-MβCD complex treated or untreated host cells were allowed to bind 0.1% labeled RBC suspension for 10 min at 30°C. Fluorescence and Nomarski images of cells within the same microscope field before and after lowering pH were acquired (SIT video camera [Dage MTI] and NIH ImageJ software). Additional images of dye mixing were recorded at five randomly selected microscope fields of the same dish.

Image Acquisition and Data Analysis

Fluorescence images (movies) of low pH–triggered dye transfer from labeled RBC to HAS cells were recorded with a Cascade 512B camera (Roper Scientific, exposure time 10 ms, binning 4; 30,000 frames). Image frames were captured and analyzed using IPLab 3.6 (Scanalytic Inc.) software. Fluorescence intensity (F) of Alexa 10-kD dextran or CF were measured in regions of interest (ROI) in the center of HAS cells with a fixed area (35,904 pixels). For DiI, fluorescence intensities were measured in a smaller ROI (896 pixels). The mean plateau intensity (F_P) and mean base intensity (F_0) were measured in the given ROI and normalized according to the formula $[(F - F_0)/(F_P - F_0)] \times 100$. When comparing the extent of fusion between cholesterol-treated and untreated cells, the whole HAS-RBC cell pair was included in a large ROI (144,768 pixels). The highest observed value of F_P of a cholesterol-treated cell was converted to 100% and percent relative fluorescence intensities (%RFI) were measured compared to this 100% value. Fluorescent dye waiting time was the measured duration between the pH trigger pulse (marked with a visible light pulse) and initiation of dye distribution (mean F above F_0).

To control for cholesterol-induced changes in HAS cell lipid dye diffusion per se, we estimated the difference in dye propagation across the HAS cell after fusion, with and without cholesterol enrichment, by putting two spot regions of interest (ROI) close to and distal from the fusion junction. The estimated time difference in dye propagation between the two points within the HAS cell membranes do not differ with cholesterol treatment (not depicted). Thus, cholesterol facilitated early dye transfer from the RBC without affecting dye diffusion within the HAS cell membrane.

Electrophysiological Measurements

HAS-RBC cell pairs in solution of (in mM) 150 *N*-methylglucamine succinate, 5 $MgCl_2$, 2 Cs-HEPES (pH 7.2) were patched with ~2–3 MΩ pipettes filled with (in mM) 155 Cs-glutamate, 5 $MgCl_2$, 5 1,2-bis(2-aminophenoxy)ethane-*N,N,N,N*-tetraacetic acid, and 10 Cs-HEPES (pH 7.4). In the whole cell configuration, admittance recording were made with an EPC 7 patch-clamp amplifier (List-Medical), and the data were recorded with a software-based lock-in amplifier, Browse (Ratinov et al., 1998) using a sine wave (f = 1000 Hz, ± 15 mV peak to peak) superimposed on a +10 to −10 mV holding potential. Fusion pore conductance, G_{Pore} was calculated off-line from changes in G_{DC}, G_{AC}, and C_{RBC} using the software Browse (Ratinov et al., 1998).

Analysis of Experimental Data

Sigma Plot (SPSS Inc.) was used for all analyses. Data are presented as the mean ± SEM with the number of experiments, *n* = number, listed. Sample means were compared using the unpaired Student's *t* test and the level of significance, P, indicated.

Online Supplemental Materials

The online supplemental material (available at http://www.jgp.org/cgi/content/full/jgp.200709932/DC1) contain two movies showing a difference in the extent of fusion between untreated and cholesterol-treated pairs. Video 1 shows that in untreated pairs the RBC did not completely fuse with the HAS cell membrane with full content (CF) mixing. Video 2 shows that with increased cholesterol, not only did the bound RBC completely release their lumenal contents to HAS cells, but the membrane of the target RBC flattened and completely collapsed into the curve of the cholesterol-enriched HAS cell membrane.

RESULTS

HAS Cell Cholesterol Level and Fusion Activity

HAS cells are Sf9 insect cells that stably express HA in their plasma membrane, as demonstrated by flow cytometry, cell surface biotinylation, and immunoblot assays (see Materials and methods). When fusion is triggered by lowering the pH in the extracellular solution, lipidic and aqueous dyes can transfer from bound, doubly labeled RBC to HAS cells; lipid dye transfer is consistent with membrane outer leaflet merger, and aqueous dye transfer is consistent with pore opening and fusion. At pH 4.9 and 30°C, 74 ± 4% (n = 21) of bound cells show lipid dye transfer within 10 min after lowering pH, while only 35 ± 3% (n = 21) show aqueous dye transfer (Fig. 3). When HAS cells were enriched with cholesterol using

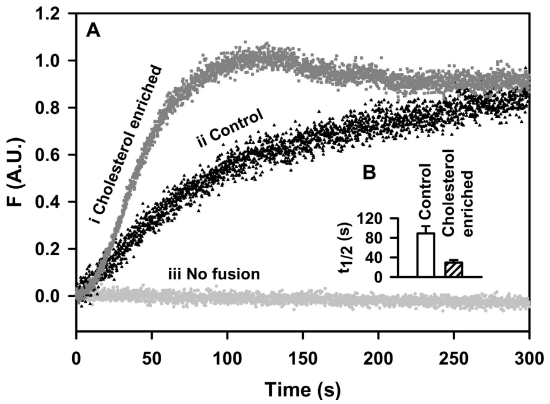

Figure 4. Cholesterol affects lipid mixing. Lowering pH initiated diffusion of lipid dye from the RBC to the HAS cell membrane. (A) Changes in fluorescence intensity (F) were measured in a small ROI at the periphery of HAS cells opposite to site of the bound of RBC using a fixed area (896 pixel). Cholesterol enrichment led to faster lipid dye transfer (i) compared with untreated cells (ii). In i and ii time zero is the onset of dye diffusion and iii is the F measurement of an unfused cell pair. (B) Time required to reach half-maximum fluorescence ($n > 5$).

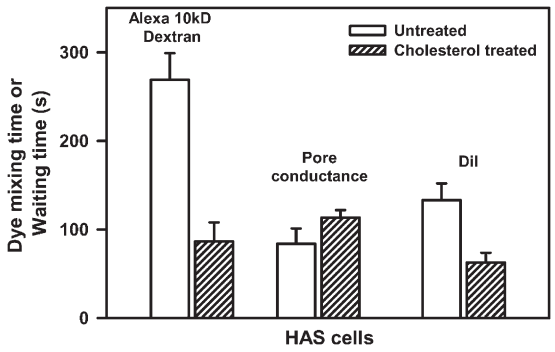

Figure 5. Cholesterol enrichment affects dye distribution time. Dye distribution time for Alexa 10 kD dextran and DiI were measured as the time between pH trigger and the onset of dye distribution (mean F above F_0). Waiting times were measured as the interval of time between pH trigger and the electrophysiological detection of fusion pore conductance ($n > 5$).

MβCD (see Materials and methods), there was a significant increase in aqueous dye transfer compared to untreated control (73 ± 3%, $P < 0.005$, $n = 15$, Fig. 3) with comparable lipid dye transfer (84 ± 3%, $P < 0.08$, $n = 15$). Thus, increasing cholesterol in the host cell significantly increased fusion (aqueous dye transfer) but did not affect membrane merger (lipid dye transfer).

Sub-optimal Fusion Conditions Reveal Differential Effects with Cholesterol and Oleic Acid

To determine if the cholesterol sensitivity for fusion had the same locus as another lipid-sensitive stage, the stalk, we compared cholesterol treatment with the stalk-promoting agent oleic acid (Chernomordik et al., 1997, 1998). Indeed, when oleic acid was added to HAS-RBC cell pairs (10 min preincubation with soluble oleic acid and MβCD) and then cell pairs were triggered with pH 4.9, there was a significant increase in aqueous dye transfer compared to untreated control (71 ± 5%, $n = 5$, $P < 0.005$, Fig. 3) with comparable lipid dye transfer (89 ± 3%, $n = 5$, $P < 0.09$, Fig. 3). To better probe the effect of oleic acid on the stalk, suboptimal conditions were chosen to make lipid mixing the rate limiting step: at pH 5.3 and 30°C, 45 ± 11% ($n = 4$) of bound cells show lipid dye transfer (Fig. 3). Under these suboptimal conditions, cholesterol-enriched HAS cells triggered at pH 5.3 show no significant increase in aqueous dye transfer compared to untreated control (17 ± 3%, $n = 6$, $P < 0.1$, Fig. 3) while comparable lipid dye transfer is observed (61 ± 4%, $n = 6$, $P < 0.3$, Fig. 3). However, oleic acid significantly increased both aqueous and lipid dye transfer compared to untreated control (38 ± 3%, $n = 5$, $P < 0.004$ and 85 ± 3%, $n = 5$, $P < 0.007$, Fig. 3). Differential effects of cholesterol and oleic acid at suboptimal fusion conditions were observed.

Cholesterol Interacts with the HA Transmembrane Domain

GPI-anchored membrane proteins are integral cell surface membrane glycoproteins that are not attached to the plasma membrane by a TMD, but by a glycosylated inositolphospholipid linked to the protein's C terminus. Since cholesterol increased aqueous dye transfer at pH 4.9, we tested if cholesterol could reverse the block of aqueous dye transfer observed with glycosylphosphatidylinositol-HA (GPI-HA) (Kemble et al., 1994; Melikyan et al., 1995; Markosyan et al., 2000). Another stable cell line expressing GPI-HA (GPIHAS) was created. The density of GPI-HA, determined by flow cytometry, was similar to that of HAS cells. Upon pH 4.9 application, GPIHAS showed lipid dye transfer (45 ± 4%, $n = 6$) but no aqueous dye transfer was observed. After enriching GPIHAS with cholesterol, lipid dye transfer remained unchanged (52 ± 8%, $n = 6$) and no aqueous dye transfer was observed (Fig. 3). The cholesterol-induced increase in HA-mediated fusion at pH 4.9 required an intact HA TMD. Cholesterol could not overcome the fusion defect of a lipidic membrane anchored HA that lacks the TMD.

Cholesterol Affects the Kinetics of Lipid Mixing and Pore Opening

Following a low pH trigger to an RBC-HAS cell pair, the first fusion events follow with a delay of usually several seconds to minutes. This delay is believed to arise from both the time required for conformational changes in the HA molecule to occur and the kinetics of fusion intermediates prior to pore opening. Faster lipid dye transfer kinetics were observed following cholesterol enrichment (Fig. 4, compare i with ii), particularly at the onset of lipid mixing. From the onset of lipid dye transfer, 89 ± 15 s ($n = 5$) was required to reach half maximum fluorescence in control cells; this time decreased significantly in cholesterol-enriched cells (29 ± 5 s, $n = 6$, $P < 0.003$, Fig. 4 B). In untreated HAS cells, DiI

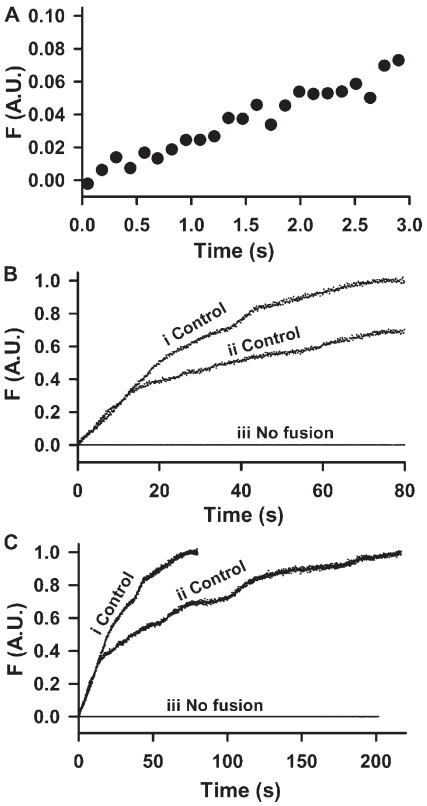

Figure 6. Dye transfer in HAS–RBC cell pair fusion. Images of HAS–RBC cell pair fusion were captured. pH triggering initiated dye transfer (CF) from the RBC to the HAS cell lumen, and changes in fluorescence intensity (F) were measured in regions of interest (ROI) with a fixed area (35,904 pixel) near the centers of the HAS cells. Time 0 represents the onset of dye transfer. (A) Changes in F of the CF dye, compared to background, can be detected with good time resolution. (B) Two examples of untreated cell pairs with considerable variability in their F kinetics. In one HAS cell, the F increases monotonically to a plateau (i), but the F increase may also be irregular, with different F rates until a plateau is reached (ii). (C) The same two examples on a longer time scale.

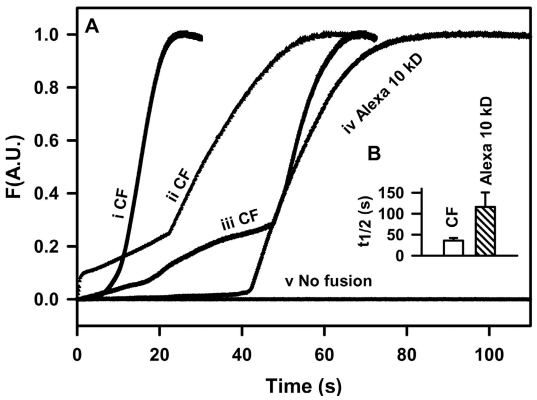

Figure 7. Cholesterol enrichment change HAS cell fusion kinetics. Changes in fluorescence intensity (F) were measured in the region of interest (ROI) near the center of HAS cells with a fixed area (35,904 pixel). HAS cells were enriched with cholesterol by standard incubation with soluble cholesterol-MβCD complex. (A, i–iii) Different kinetic phases are observed with CF transfer. (iv) Transfer of Alexa 10 kD dextran was initially slow, but then showed faster kinetics. In i–iv, time zero is the onset of dye diffusion. F measurement of an unfused cell pair is in v. (B) Time required to reach half-maximum fluorescence (n >7).

transfer across the cell membrane occurred in 133 ± 19 s (n = 8) following the pH trigger (Fig. 5). In contrast, DiI transfer across the cell membrane was significantly faster in cholesterol-treated HAS cells following pH trigger (48 ± 5 s, n = 11, P < 0.004, Fig. 5).

The delay in pore opening was compared using an aqueous dye and electrophysiology. Untreated HAS cells fusing with RBC ghosts containing 10-kD Alexa dextran required 269 ± 30 s (n = 7) after pH trigger to detect the fluorescence change in the lumen of the HAS cells (Fig. 5). In contrast, the fluorescence change observed in cholesterol-treated HAS cells occurred in 86 ± 21 s (n = 8) after pH trigger (Fig. 5). However, the duration between the pH trigger and pore opening, the waiting time, measured with time-resolved whole-cell admittance patch clamp technique (Ratinov et al., 1998) in HAS cells was 89 ± 17 s (n = 9) (Fig. 5) and did not change significantly upon cholesterol enrichment (113 ± 8 s, n = 4). In untreated HAS cells there exist fusion pores that are too small to be detected by 10-kD dye transport. However, following cholesterol treatment, these fusion pores can be detected by 10-kD dye transport.

Cholesterol Affects the Initial State of the Fusion Pore

Formation of a fusion pore is the earliest detectable post fusion event. In Fig. 6 (A–C), fluorescence changes are plotted over three different time scales. Fluorescence microscopy of single cell pairs of untreated HAS bound to 370 D carboxy fluorescein (CF)–loaded RBC showed that CF has subsecond access to the HAS lumen upon fusion (Fig. 6 A). Control cells have considerable variability in their fluorescence intensity (F) kinetics (Fig. 6, B and C). Control HAS cell fluorescence increased to a plateau with variable times (e.g., Fig. 6 B i and Fig. 6 C ii). In addition, untreated cells have considerable variability in their fluorescence intensity (F) kinetics, with irregular and occasionally slow increases in F prior to reaching a plateau (Fig. 6 C ii).

In contrast, upon cholesterol enrichment, at least three distinct F kinetics phases were observed (Fig. 7): (1) 75% of the cholesterol enriched kinetics showed a rapid rise to a maximum (e.g., Fig. 7 A, i CF), (2) an initially rapid increase, interrupted momentarily by a period of slower increase, and then an increased rate (Fig. 7 A, ii CF), and (3) a "foot," lasting up to several seconds, preceding a faster rise in F (Fig. 7 A, iii CF). The last two groups comprised 25% of the observed kinetics. Since the gradient of dye is expected to not change much initially, these changes in dye flux most likely reflect transitions in the aggregate aqueous space between the fusing cells, i.e., the fusion pore region. These transitions are consistent with changes

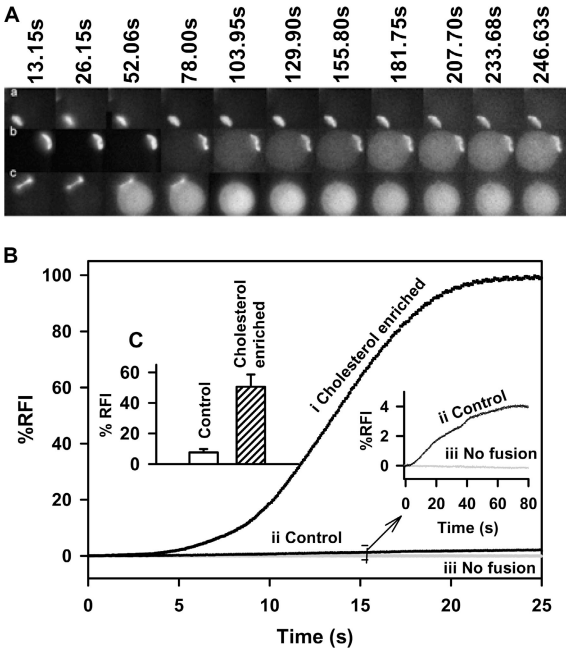

Figure 8. Cholesterol affects the extent of fusion. (A) Fluorescence images of a CF-labeled RBC fusing to a HAS cell. (a) Frames of unfused cell pair. (b) Low pH–triggered (pH trigger at $t = 0$, not shown in the picture) HAS–RBC cell pair fusion. Fluorescent dye remains trapped in RBC at the end of acquisition. (c) Fusion of cholesterol-enriched HAS cells. Target RBC membrane completely merged with cholesterol-enriched HAS cell membrane. (B) Comparison of the plateau phase of dye transfer. Entire HAS-RBC cell pairs were included in the ROI and F were compared relative to baseline fluorescence $[(F - F_0)/(F_P - F_0)] \times 100$. F were then compared with the highest intensity of the plateau phase and expressed as percentage relative fluorescence intensity (%RFI). (B, i) Dye transfer in cholesterol-enriched HAS cells. (ii) Dye transfer in untreated HAS cells is slow and RFI increases to only ~4% compared to cholesterol enriched HAS cells. In i and ii, time zero is the onset of dye transfer. (iii) Relative fluorescence intensity (RFI) measurement of unfused cell pair. (C) Bar chart showing %RFI of cholesterol-enriched HAS cells (with pattern) and control or untreated HAS cells ($n > 7$).

in both fusion pore number and fusion pore size (width and length). With 10-kD Alexa dye, a slow F increase was observed, which then increased rapidly (Fig. 7 A, iv Alexa 10 kD); this kinetic behavior is consistent with the presence of an initially small aqueous space undergoing a transition to a larger aqueous space. This interpretation is consistent with the differences in the time to reach half maximum fluorescence after pH trigger, for both dyes. CF required 36 s ± 5 s ($n = 8$) to reach half the maximum fluorescence, and this time is significantly increased ($P < 0.04$) to 116 ± 34 s ($n = 7$) when dye size is increased to 10 kD (Fig. 7 B).

Cholesterol Affects Fusion Phenotype and/or Extent of Fusion

There was a morphological difference between untreated and cholesterol-treated cell pairs following fusion. In untreated HAS-RBC pairs, the RBC did not completely fuse into the HAS cell membrane with full content transfer and complete incorporation of the RBC membrane (Fig. 8). The two distinct compartments (HAS and RBC) remained separate throughout the experiment (Fig. 8 A). Even under conditions when some dye was presumably released (see 78 s in Fig. 8 A, b), dye was retained in the RBC and observed at the end of the acquisition time (247 s; also see Video 1, available at http://www.jgp.org/cgi/content/full/jgp.200709932/DC1). With cholesterol treatment, not only did bound RBC completely transfer their lumenal contents into HAS cells (see 103.95 s in Fig. 8 A, c), but the membrane of the target RBC flattened (see Video 2) and completely collapsed into the surface of the cholesterol-enriched HAS cell membrane, suggesting syncytium formation following opening of the fusion pore (Fig. 8 A, c). Thus, the presence of cholesterol allowed the fusion pathway to go to completion; collapse of the RBC membrane into the HAS cell membrane.

To parameterize the extent of fusion pore development, the increase from baseline in aqueous F relative to its maximum value observed during the experiment was measured. A typical example (Fig. 8 B, i) shows an ~25-fold increase in percentage relative fluorescence intensity (%RFI) in cholesterol-treated HAS cells compared to untreated cells (Fig. 8 B, ii). The mean extent of increase in %RFI in HAS cells was 7.6 ± 2.2% ($n = 7$) compared with 50.6 ± 8.0% ($n = 9$) in cholesterol-treated HAS cells (Fig. 8 C). Thus, the effect of cholesterol on the fusion pore is at the late phases of pore expansion where the size of the aqueous space between the fusing cells is controlled.

Cholesterol Widens the Fusion Pore

We further tested whether fusion pore expansion, as measured electrically at the single pore level, was affected by cholesterol. HAS-RBC cell pairs were patched in the whole cell configuration. In both cholesterol-enriched and control HAS cells, the size of the initial fusion pore is not significantly different (0.30 ± 0.09 nS [$n = 4$] and 0.50 ± 0.05 nS [$n = 9$], respectively, $P < 0.9$, Fig. 9 A). In the absence of cholesterol, lipid dye transfer and capacitance steps (Fig. 9 B) were observed. In the first few milliseconds of the initial fusion pore opening, the pore conductance (G_{Pore}) did not increase steadily, but capacitance gradually increased by steps to ~1.25 pF, which is equivalent to the membrane capacitance of RBC (Fig. 9 B). In contradistinction, upon cholesterol enrichment G_{Pore} increased after each step in pore conductance (Fig. 9 C). The slope of G_{Pore}, after each step in pore conductance, was measured and used to estimate pore expansion. Control cell pairs had a conductance rate of 3.9 ± 1.2 nS/s ($n = 5$), which is significantly ($P < 0.004$) lower than the 8.2 ± 1.7 nS/s ($n = 4$) conductance rate observed in cholesterol-enriched cells (Fig. 9 C). Additionally, in the absence of cholesterol, the time course of G_{Pore} over seconds was

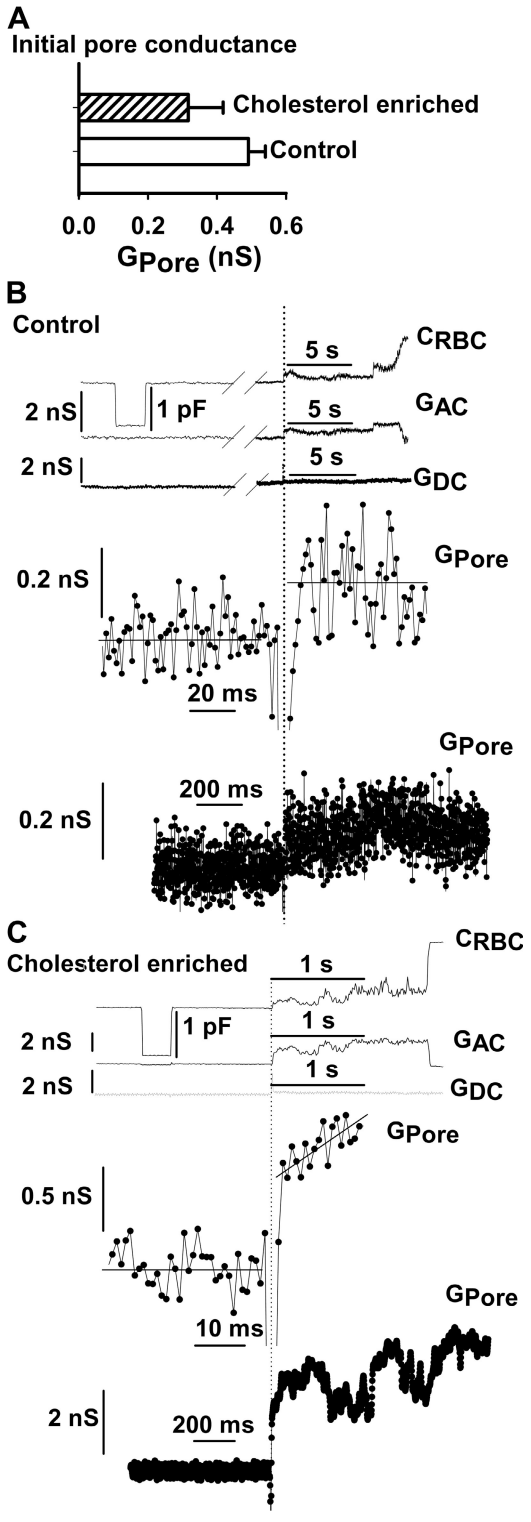

Figure 9. Fusion pore analysis. Initial fusion pore conductance (A) and fusion pore opening recorded by patch clamp electrophysiology in (B) untreated and (C) cholesterol-enriched HAS cells. The components of admittance are cell membrane capacitance (C_{RBC}), AC conductance (G_{AC}), DC conductance (G_{DC}), and fusion pore conductance (G_{Pore}). Fusion pore conductances, G_{Pore}, were calculated offline from G_{AC}, G_{DC}, and C_{RBC} using software Browse (Ratinov et al., 1998). In HAS cells, the initial fusion pore is small ~0.2 nS and pore growth is stunted. In cholesterol-enriched HAS cells, fusion pores enlarge, indicating that cholesterol promotes pore expansion ($n \geq 4$). The vertical dotted line represents fusion pore opening.

consistent with a stunted fusion pore (Fig. 9 B) while an expanding fusion pore was observed in the presence of cholesterol (Fig. 9 C).

DISCUSSION

Specific intermediates of membrane fusion, catalyzed by the influenza virus protein hemagglutinin, are regulated by cholesterol. The extent of early lipid transfer in Sf9 cells expressing HA (HAS cells) is similar to that previously observed in mammalian cell systems (Chernomordik et al., 1997, 1998), but the initial fusion pore is small and pore expansion is stunted. A three-fold increase in cellular cholesterol (see Materials and methods) leads to (a) faster lipid dye transfer kinetics, (b) increased amount of aqueous dye transferred, (c) increased extent of aqueous dye transferred, and (d) an increase in the rate of pore conductance. The cholesterol-dependent increase in fusion efficiency required an intact HA TMD and optimal pH. Overall, these results support the hypothesis that host cell cholesterol acts at two stages in membrane fusion: (1) an early, lipidic stage prior to fusion pore opening and (2) a later stage during fusion pore expansion. How can the physical properties of cholesterol influence fusion?

Pore Expansion

Cholesterol increases the extent of aqueous dye transferred (Fig. 8, A and B), suggesting a role in pore expansion. The amount of dye transferred from labeled RBC increased 25-fold upon cholesterol treatment (Fig. 8 B); this observation is consistent with the pore widening observed in treated cells using capacitance measurements. These results suggest that in control HAS cells, small, multiple pores form but remain too small to conduct a 370 D dye. Furthermore, pore conductance measurements can distinguish between pore opening and expansion. Between pore conductance steps, reflecting the opening of new pores, a steady increase in the rate of conductance is indicative of pore expansion (Scepek et al., 1998). In control cells the slope of pore conductance was low (Fig. 9 B), yet the appearance of continual stepwise increases in conductance is consistent with the opening of multiple, nonexpanding pores ~0.2–0.5 nS in size (Zimmerberg et al., 1994). With cholesterol-enriched cells, the slope was higher and the number of resolvable steps decreased (Fig. 9 C), suggesting the formation of fewer, but expanding pores. The increased conductance rate observed with cholesterol enrichment, similar to high cholesterol–containing mammalian cells (Spruce et al., 1989; Zimmerberg et al., 1994;

Melikyan et al., 1995; Frolov et al., 2003), indicated that cholesterol is a major determinant in the expansion of pores in HA-mediated fusion.

Cholesterol Head Group Condensation in the Pre-pore Stage

According to one model, a very small "pre-pore" forms prior to the detection of the smallest fusion pores (Kuzmin et al., 2001). The pre-pore is facilitated by lipids of negative spontaneous monolayer curvature such as cholesterol (Kuzmin et al., 2001). In the pre-pore structure, the trans monolayers have merged and create the narrowest aqueous pathway between the two compartments. Since the pore radius has not yet expanded beyond that of the modified stalk, the acyl chains of both monolayers are compressed, predominantly in the equatorial region. In this stage, cholesterol molecules are hypothesized to fit well in the equatorial region and could stabilize the pre-pore structure by head group condensation. The pre-pore spontaneously expands to a true fusion pore; free energy decreases with increasing radius because of decompression, and decreased lipid bending and tilting. Thus, two of cholesterol's features observed in model systems, negative spontaneous monolayer curvature and head group condensation (Schmidt et al., 1977; Boggs, 1980), could play a key role in these fusion intermediates.

Interactions between Cholesterol and the TMD of HA

The effect of cholesterol on pore expansion could occur through changes in a global membrane property, and/or through localized interactions of lipids around a fusion pore, and/or through specific interaction with the HA TMD. Specific interaction with HA TMD can be ruled out if (a) the effect of cholesterol on fusion is seen without the TMD or if (b) cholesterol modulation of the pore is not unique to HA. To address the first point, our results with GPI-HAS (HAS cells without a complete TMD) demonstrate that regulation by cholesterol required a TMD. GPI-HAS, which has a short glycophophatidylinositol lipid anchoring it to the membrane instead of a full-length transmembrane domain, transfers lipid dye but not aqueous dye upon pH triggering; this is similar to mammalian cell lines expressing GPI-HA (Armstrong et al., 2000; Frolov et al., 2000; Melikyan et al., 2000) where cholesterol enrichment of these cells could not rescue complete fusion (Fig. 3). Thus, the requirement for an intact HA TMD does not support the hypothesis that cholesterol regulation is a purely lipidic phenomenon, like the membrane destabilizing effect of cholesterol on PC/PE planar membranes in the absence of sphingomyelin (Cullis and de Kruijff, 1979), which leads to rupture and fusion pore opening.

To address the second point, we note that fusion protein GP64-expressing Sf9 cells form an expanding pore when fusing to RBC (Plonsky and Zimmerberg, 1996). Thus, cholesterol is not initially needed in the cell expressing HA to obtain expanding fusion pores using the same Sf9 cell line; presumably cholesterol equilibrates rapidly once an initial fusion intermediate such as the stalk forms. Between Sf9 cells, only with cholesterol enrichment does one obtain expanding fusion pores. Moreover, in mammalian cells, which have ~40 mole % cholesterol, HA-mediated pores are exclusively of the expanding type (Spruce et al., 1989; Zimmerberg et al., 1994; Melikyan et al., 1995; Frolov et al., 2003), whereas GPI-HA pores are stunted. Thus, the interaction of the HA TMD with cholesterol may be important in determining the mechanism of cholesterol action. Indeed, point mutations on the TMD of HA affect the detergent solubility and intracellular trafficking of HA (Simons and Ikonen, 1997; Lin et al., 1998; Scheiffele et al., 1997, 1999).

Cholesterol as a Modulator of Membrane Phase Behavior

The fact that cholesterol increases all quantifiable parameters of membrane fusion, including kinetics, is also consistent with a role of cholesterol to increase the mobility of HA in the plane of the membrane. There are two ways this could happen: (1) a decrease in fluid membrane viscosity with increasing membrane cholesterol and (2) a change in the phase behavior of the cell membrane, to increase the fraction of lipids that are fluid. In support of the second possibility, recent NMR data from the influenza envelope shows a considerable fraction of the lipids to be in the gel phase at room temperature, coexisting with liquid ordered and disordered lipids (Polozov et al., 2008). In fact, decreasing cholesterol in this system reversibly increased the fraction of gel lipids at room temperature. Thus the HA trimers that form the initial fusion pore by scaffolding lipids may not be able to move radially outward to allow the fusion pore to expand.

Conclusion

We have shown that cholesterol promotes both lipid transfer (hemi-fusion) and fusion pore expansion in the cell–cell membrane fusion mediated by influenza HA. The cholesterol effect requires a complete TMD and optimal pH. We hypothesize that cholesterol promotes fusion pore expansion by (a) virtue of its negative intrinsic curvature and (b) the same specific cholesterol/lipid/HA interactions that mediate the 1–10-nm scale clustering of HA in the plane of the membrane (Hess et al., 2005), the mobility of HA in fibroblasts (Hess et al., 2007), and the phase behavior of the influenza envelope (Polozov et al., 2008). These structural forces act at the fusion stage of viral invasion to facilitate fusion pore widening.

We would like to thank Dr. Jean-Charles Grivel (NICHD, NIH) for his help with FACS experiments.

This work was supported by the intramural program of the National Institute of Child Health and Human Development, National Institutes of Health.

Olaf S. Andersen served as editor.

Submitted: 28 November 2007
Accepted: 2 April 2008

REFERENCES

Armstrong, R.T., A.S. Kushnir, and J.M. White. 2000. The transmembrane domain of influenza hemagglutinin exhibits a stringent length requirement to support the hemifusion to fusion transition. *J. Cell Biol.* 151:425–437.

Ashbourne Excoffon, K.J., T. Moninger, and J. Zabner. 2003. The coxsackie B virus and adenovirus receptor resides in a distinct membrane microdomain. *J. Virol.* 77:2559–2567.

Bavari, S., C.M. Bosio, E. Wiegand, G. Ruthel, A.B. Will, T.W. Geisbert, M. Hevey, C. Schmaljohn, A. Schmaljohn, and M.J. Aman. 2002. Lipid raft microdomains: a gateway for compartmentalized trafficking of Ebola and Marburg viruses. *J. Exp. Med.* 195:593–602.

Boggs, J.M. 1980. Intermolecular hydrogen bonding between lipids: influence on organization and function of lipids in membranes. *Can. J. Biochem.* 58:755–770.

Brown, D.A., and E. London. 1998. Functions of lipid rafts in biological membranes. *Annu. Rev. Cell Dev. Biol.* 14:111–136.

Chazal, N., and D. Gerlier. 2003. Virus entry, assembly, budding, and membrane rafts. *Microbiol. Mol. Biol. Rev.* 67(2):226–237.

Chernomordik, L. 1996. Non-bilayer lipids and biological fusion intermediates. *Chem. Phys. Lipids.* 81:203–213.

Chernomordik, L., E. Leikina, V. Frolov, P. Bronk, and J. Zimmerberg. 1997. An early stage of membrane fusion mediated by the low pH conformation of influenza hemagglutinin depends upon membrane lipids. *J. Cell Biol.* 136:81–93.

Chernomordik L, V.A. Frolov, E. Leikina, P. Bronk, and J. Zimmerberg. 1998. The pathway of membrane fusion catalyzed by influenza hemagglutinin: restriction of lipids, hemifusion, and lipidic fusion pore formation. *J. Cell Biol.* 140:1369–1382.

Chizmadzhev, Y.A., F.S. Cohen, A. Shcherbakov, and J. Zimmerberg. 1995. Membrane mechanics can account for fusion pore dilation in stages. *Biophys. J.* 69(6):2489–2500.

Christian, A.E., M.P. Haynes, M.C. Phillips, and G.H. Rothblat. 1997. Use of cyclodextrin for manipulating cellular cholesterol content. *J. Lipid Res.* 38:2264–2272.

Churchward, M.A., T. Rogasevskaia, J. Höfgen, J. Bau, and J.R. Cooressen. 2005. Cholesterol facilitates the native mechanism of Ca^{2+}-triggered membrane fusion. *J. Cell Sci.* 118:4833–4848.

Churchward, M.A., T. Rogasevskaia, D.M. Brandman, H. Khosravani, P. Nava, J.K. Atkinson, and J.R. Coorssen. 2008. Specific lipids supply critical intrinsic negative curvature—an essential component of native Ca^{2+}-triggered membrane fusion. *Biophys. J.* doi:10.1529/biophysj.107.123984.

Cullis, P.R., and B. de Kruijff. 1979. Lipid polymorphism and the functional roles of lipids in biological membranes. *Biochim. Biophys. Acta.* 559:399–420.

Danieli, T., S.L. Pelletier, Y.I. Henis, and J.M. White. 1996. Membrane fusion mediated by the influenza virus hemagglutinin requires the concerted action of at least three hemagglutinin trimers. *J. Cell Biol.* 133:559–569.

Del Real, G., S. Jimenez-Baranda, R.A. Lacalle, E. Mira, P. Lucas, C. Gomez-Mouton, A.C. Carrera, A.C. Martinez, and S. Manes. 2002. Blocking of HIV-1 infection by targeting CD4 to nonraft membrane domains. *J. Exp. Med.* 196:293–301.

Edidin, M. 2003. The state of lipid rafts: from model membranes to cells. *Annu. Rev. Biophys. Biomol. Struct.* 32:257–283.

Ellens, H., S. Doxsey, J.S. Glenn, and J.M. White. 1989. Delivery of macromolecules into cells expressing a viral membrane fusion protein. *Methods Cell Biol.* 31:155–178.

Feigenson, G.W., and J.T. Buboltz. 2001. Ternary phase diagram of dipalmitoyl-PC/dilauroyl-PC/cholesterol: nanoscopic domain formation driven by cholesterol. *Biophys. J.* 80:2775–2788.

Fridriksson, E.K., P.A. Shipkova, E.D. Sheets, D. Holowka, B. Baird, and F.W. McLafferty. 1999. Quantitative analysis of phospholipids in functionally important membrane domains from RBL-2H3 mast cells using tandem high-resolution mass spectrometry. *Biochemistry.* 38:8056–8063.

Frolov, V.A., M.S. Cho, P. Bronk, T.S. Reese, and J. Zimmerberg. 2000. Multiple local contact sites are induced by GPI-linked influenza hemagglutinin during hemifusion and flickering pore formation. *Traffic.* 1:622–630.

Frolov, V.A., A.Y. Dunina-Barkovskaya, A.V. Samsonov, and J. Zimmerberg. 2003. Membrane permeability changes at early stages of influenza hemagglutinin-mediated fusion. *Biophys. J.* 85(3):1725–1733.

Gimpl, G., U. Klein, H. Reiländer, and F. Fahrenholz. 1995. Expression of the human oxytocin receptor in baculovirus-infected insect cells: high-affinity binding is induced by a cholesterol-cyclodextrin complex. *Biochemistry.* 34:13794–13801.

Guyader, M., E. Kiyokawa, L. Abrami, P. Turelli, and D. Trono. 2002. Role for human immunodeficiency virus type 1 membrane cholesterol in viral internalization. *J. Virol.* 76:10356–10364.

Haque, M.E., T.J. McIntosh, and B.R. Lentz. 2001. Influence of lipid composition on physical properties and peg-mediated fusion of curved and uncurved model membrane vesicles: "nature's own" fusogenic lipid bilayer. *Biochemistry.* 40:4340–4348.

Harder, T., P. Scheiffele, P. Verkade, and K. Simons. 1998. Lipid domain structure of the plasma membrane revealed by patching of membrane components. *J. Cell Biol.* 141:929–942.

Hess, S.T., M. Kumar, A. Verma, J. Farrington, A. Kenworthy, and J. Zimmerberg. 2005. Quantitative electron microscopy and fluorescence spectroscopy of the membrane distribution of influenza hemagglutinin. *J. Cell Biol.* 169:965–976.

Hess, S.T., T.J. Gould, M.V. Gudheti, S.A. Maas, K.D. Mills, and J. Zimmerberg. 2007. Dynamic clustered distribution of hemagglutinin resolved at 40 nm in living cell membranes discriminates between raft theories. *Proc. Natl. Acad. Sci. USA.* 104:17370–17375.

Huang, J., and G.W. Feigenson. 1999. A microscopic interaction model of maximum solubility of cholesterol in lipid bilayers. *Biophys. J.* 76:2142–2157.

Keller, P., and K. Simons. 1998. Cholesterol is required for surface transport of influenza virus hemagglutinin. *J. Cell Biol.* 140:1357–1367.

Kemble, G.W., T. Danieli, and J.M. White. 1994. Lipid-anchored influenza hemagglutinin promotes hemifusion, not complete fusion. *Cell.* 76:383–391.

Kenworthy, A.K., N. Petranova, and M. Edidin. 2000. High-resolution FRET microscopy of cholera toxin B-subunit and GPI-anchored proteins in cell plasma membranes. *Mol. Biol. Cell.* 11:1645–1655.

Kielian, M.C., and A. Helenius. 1984. Role of cholesterol in fusion of Semliki forest virus with membranes. *J. Virol.* 52:281–283.

Kozak, S.L., J.M. Heard, and D. Kabat. 2002. Segregation of CD4 and CXCR4 into distinct lipid microdomains in T lymphocytes suggests a mechanism for membrane destabilization by human immunodeficiency virus. *J. Virol.* 76:1802–1815.

Kozlov, M.M., S.L. Leikin, L.V. Chernomordik, V.S. Markin, and Y.A. Chizmadzhev. 1989. Stalk mechanism of vesicle fusion. Intermixing of aqueous contents. *Eur. Biophys. J.* 17:121–129.

Kozlovsky, Y., and M.M. Kozlov. 2003. Membrane fission: model for intermediate structures. *Biophys. J.* 85:85–96.

Kretzschmar, E., K. Kuroda, and H.D. Klenk. 1995. Baculovirus expression protocols. *In* Methods in Molecular Biology. Vol. 39. C.D. Richardson, editor. Humana Press, New Jersey. 317–336.

Kuzmin, P.I., J. Zimmerberg, Y.A. Chizmadzhev, and F.S. Cohen. 2001. A quantitative model for membrane fusion based on low-energy intermediates. *Proc. Natl. Acad. Sci. USA.* 98:7235–7240.

Latham, T., and J.M. Galarza. 2001. Formation of wild-type and chimeric influenza virus-like particles following simultaneous expression of only four structural proteins. *J. Virol.* 75:6154–6165.

Lin, S., H. Y. Naim, C. Rodriguez, and M. Roth. 1998. Mutations in the middle of the transmembrane domain reverse the polarity of transport of the influenza virus hemagglutinin in MDCK epithelial cells. *J. Cell Biol.* 142:51–57.

Marheineke, K., S. Grünewald, W. Christie, and H. Reiländer. 1998. Lipid composition of *Spodoptera frugiperda* (Sf9) and *Trichopulsia ni* (Tn) insect cells used for baculovirus infection. *FEBS Lett.* 441:49–52.

Markin, V.S., M.M. Kozlov, and V.L. Borovjagin. 1984. On the theory of membrane fusion. The stalk mechanism. *Gen. Physiol. Biophys.* 3:361–377.

Markosyan, R.M., F.S. Cohen, and G.B. Melikyan. 2000. The lipid-anchored ectodomain of influenza virus hemagglutinin (GPI-HA) is capable of inducing nonenlarging fusion pores. *Mol. Biol. Cell.* 11:1143–1152.

McGee, T.P., H.H. Cheng, H. Kumagai, S. Omura, and R.D. Simoni. 1996. Degradation of 3-hydroxy-3-methylglutaryl-CoA reductase in endoplasmic reticulum membranes is accelerated as a result of increased susceptibility to proteolysis. *J. Biol. Chem.* 271:25630–25638.

Melikyan, G.B., W.D. Niles, V.A. Ratinov, M. Karhanek, J. Zimmerberg, and F.S. Cohen. 1995. Comparison of transient and successful fusion pores connecting influenza hemagglutinin expressing cells to planar membranes. *J. Gen. Physiol.* 106:803–819.

Melikyan, G.B., J.M. White, and F.S. Cohen. 2000. GPI-anchored influenza hemagglutinin induces hemifusion to both red blood cell and planar bilayer membranes. *J. Cell Biol.* 131:679–691.

Nieva, J.L., R. Bron, J. Corver, and J. Wilschut. 1994. Membrane fusion of Semliki Forest virus requires sphingolipids in the target membrane. *EMBO J.* 13:2797–2804.

Ono, A., and E.O. Freed. 2001. Plasma membrane rafts play a critical role in HIV-1 assembly and release. *Proc. Natl. Acad. Sci. USA.* 98:13925–13930.

Phalen, T., and M. Kielian. 1991. Cholesterol is required for infection by Semliki Forest virus. *J. Cell Biol.* 112:615–623.

Plonsky, I., and J. Zimmerberg. 1996. The initial fusion pore induced by baculovirus GP64 is large and forms quickly. *J. Cell Biol.* 135:1831–1839.

Plonsky, I., D.H. Kingsley, A. Rashtian, P.S. Blank, and J. Zimmerberg. 2008. Initial size and dynamics of viral fusion pores are a function of the fusion protein mediating membrane fusion. *Biol. Cell.* Jan. 22 (Epub ahead of print). doi:10.1042/BC20070040.

Polozov, I. V., L. Bezrukov, K. Gawrisch, and J. Zimmerberg. 2008. Progressive ordering with decreasing temperature of the phospholipids of influenza virus. *Nat. Chem. Biol.* 4:248–255.

Popik, W., T.M. Alce, and W.C. Au. 2002. Human immunodeficiency virus type 1 uses lipid raft-colocalized CD4 and chemokine receptors for productive entry into $CD4^+$ T cells. *J. Virol.* 76:4709–4722.

Ratinov, V., I. Plonsky, and J. Zimmerberg. 1998. Fusion pore conductance: experimental approaches and theoretical algorithms. *Biophys. J.* 74:2374–2387.

Raznikov, V.I., and F.S. Cohen. 2000. Sterol and sphingolipids strongly affects the growth of fusion pores induced by the hemagglutinin of influenza virus. *Biochemistry.* 39:13462–13468.

Scepek, S., J.R. Coorssen, and M. Lindau. 1998. Fusion pore expansion in horse eosinophils is modulated by Ca^{2+} and protein kinase C via distinct mechanisms. *EMBO J.* 17:4340–4345.

Scheiffele, P., M.G. Roth, and K. Simons. 1997. Interaction of influenza virus haemagglutinin with sphingolipid-cholesterol membrane domains via its transmembrane domain. *EMBO J.* 16:5501–5508.

Scheiffele, P., A. Rietveld, T. Wilk, and K. Simons. 1999. Influenza viruses select ordered lipid domains during budding from the plasma membrane. *J. Biol. Chem.* 274:2038–2044.

Schmitt, A.P., and R.A. Lamb. 2004. Escaping from the cell: assembly and budding of negative-strand RNA viruses. *Curr. Top. Microbiol. Immunol.* 283:145–196.

Schmidt, C.F., Y. Barenholz, and T.E. Thompson. 1977. A nuclear magnetic resonance study of sphingomyelin in bilayer systems. *Biochemistry.* 16:2649–2656.

Siegel, D.P. 1999. The modified stalk mechanism of lamellar/inverted phase transitions and its implications for membrane fusion. *Biophys. J.* 76:291–313.

Simons, K., and E. Ikonen. 1997. Functional rafts in cell membranes. *Nature.* 387:569–572.

Spruce, A.E., A. Iwata, J.M. White, and W. Almers. 1989. Patch clamp studies of single cell-fusion events mediated by a viral protein. *Nature.* 342:555–558.

Stuart, A.D., H.E. Eustace, T.A. McKee, and T.D. Brown. 2002. A novel cell entry pathway for a DAF-using human enterovirus is dependent on lipid rafts. *J. Virol.* 76:9307–9322.

Sun, X., and G.R. Whittaker. 2003. Role for influenza virus envelope cholesterol in virus entry and infection. *J. Virol.* 77:12543–12551.

Suomalainen, M. 2002. Lipid rafts and assembly of enveloped viruses. *Traffic.* 3:705–709.

Takeda. M., G.P. Leser, C.J. Russell, and R.A. Lamb. 2003. Influenza virus hemagglutinin concentrates in lipid raft microdomains for efficient viral fusion. *Proc. Natl. Acad. Sci. USA.* 100:14610–14617.

Viard, M., I. Parolini, M. Sargiacomo, K. Fecchi, C. Ramoni, S. Ablan, F.W. Ruscetti, J.M. Wang, and R. Blumenthal. 2002. Role of cholesterol in human immunodeficiency virus type 1 envelope protein-mediated fusion with host cells. *J. Virol.* 76:11584–11595.

Wang, T.Y., R. Leventis, and J.R. Silvius. 2001. Partitioning of lipidated peptide sequences into liquid-ordered lipid domains in model and biological membranes. *Biochemistry.* 40:13031–13040.

White, J., and A. Helenius. 1980. pH-dependent fusion between the Semliki Forest virus membrane and liposomes. *Proc. Natl. Acad. Sci. USA.* 77:3273–3277.

Zhang, J., A. Pekosz, and R.A. Lamb. 2000. Influenza virus assembly and lipid raft microdomains: a role for the cytoplasmic tails of the spike glycoproteins. *J. Virol.* 74:4634–4644.

Zimmerberg, J., and M.M. Kozlov. 2006. How proteins produce cellular membrane curvature. *Nat. Rev. Mol. Cell Biol.* 7:9–19.

Zimmerberg, J., R. Blumenthal, M. Curran, D. Sarkar, and S. Morris. 1994. Restricted movement of lipid and aqueous dyes through pores formed by influenza hemagglutinin during cell fusion. *J. Cell Biol.* 127:1885–1894.